Mode coupling of low frequency electromagnetic waves in magnetized dusty plasmas

L. F. Ziebell, M. C. de Juli, R. S. Schneider, and V. Jatenco-Pereira

Citation: Physics of Plasmas **12**, 082102 (2005); doi: 10.1063/1.1987270
View online: http://dx.doi.org/10.1063/1.1987270
View Table of Contents: http://scitation.aip.org/content/aip/journal/pop/12/8?ver=pdfcov
Published by the AIP Publishing

Mode coupling of low frequency electromagnetic waves in magnetized dusty plasmas

L. F. Ziebell[a)]
Instituto de Física, Universidade Federal do Rio Grande do Sul, Caixa Postal 15051, CEP: 91501-970, Porto Alegre, RS, Brazil

M. C. de Juli
Instituto de Astronomia, Geofísica e Ciências Atmosféricas, Universidade de São Paulo, Rua do Matão 1226, Cidade Universitária, CEP: 05508-900, São Paulo, SP, Brazil

R. S. Schneider
Instituto de Física, Universidade Federal do Rio Grande do Sul, Caixa Postal 15051, CEP: 91501-970, Porto Alegre, RS, Brazil

V. Jatenco-Pereira
Instituto de Astronomia, Geofísica e Ciências Atmosféricas, Universidade de São Paulo, Rua do Matão 1226, Cidade Universitária, CEP: 05508-900, São Paulo, SP, Brazil

(Received 7 April 2005; accepted 7 June 2005; published online 21 July 2005)

A kinetic description is used to analyze wave propagation in dusty plasmas, taking into account the fluctuation of the charge of the dust particles due to inelastic collisions with electrons and ions. The case of propagation of waves exactly parallel to the external magnetic field and Maxwellian distributions for the electrons and ions in the equilibrium is considered, and a parametric analysis of the dispersion relation is performed. The investigation emphasizes particularly the effects of dust density, radius of dust particles, ion temperature, ratio between electron and ion temperatures, ion density, and ambient magnetic field, on the solutions of the dispersion relation. The analysis shows the possibility of occurrence of coupling between waves in the whistler branch and waves in the branch of circularly polarized waves, in the presence of the dust particles. © *2005 American Institute of Physics*. [DOI: 10.1063/1.1987270]

I. INTRODUCTION

In a recent publication we have used a kinetic description to analyze the propagation of electromagnetic waves in dusty plasmas, taking into account the fluctuation of the dust charges due to inelastic collisions with electrons and ions.[1] We have also presented a short list of references related to the subject.[2–17]

In the formulation utilized in Ref. 1, the components of the dielectric tensor depend on the frequency of inelastic collisions between ions and electrons and the dust particles. This collision frequency is momentum dependent and, in order to simplify the evaluation of momentum integrals and solve the dispersion relation, we have assumed that it could be replaced by an average over electron or ion distribution function. The formulation has been applied to the particular case of low-frequency waves propagating along the ambient magnetic field, incorporating many details which have appeared in previous publications.[1,18,19]

We have obtained results which show that, as in the case of dustless plasmas, the dispersion relation describes two different modes, identified for higher frequencies as the whistler waves and as the circularly polarized waves. In the absence of dust these two modes collapse together, for frequencies well below ion cyclotron frequency, forming the well-known branch of the Alfvén waves. In the presence of dust particles with variable charge, however, our results show that these two modes become separated. Another effect of the presence of the dust particles with variable charge is an additional damping of the Alfvén waves, which may completely override conventional Landau damping for large wavelengths. We have seen that, for small dust density, the damping of the two modes increases nearly linearly with the dust density, while for further increase of the dust density, waves in the circularly polarized branch have the damping rate further decreased, while waves in the whistler branch continue to have increased damping rates.[1] Another novel feature obtained in Ref. 1 is the occurrence of mode coupling due to the presence of dust particles, between waves in the branch of circularly polarized waves, propagating in opposite directions.

The emphasis in Ref. 1 has been on the demonstration of the effects of the presence of dust particles on the propagation and damping of low-frequency waves. A particular set of representative parameters has been chosen and kept constant along the analysis, including parameters like the magnitude of the ambient magnetic field, the temperature of the ions and the size of the dust particles. In the present paper we return to the subject, in order to perform a parametric analysis of the dispersion relation of low-frequency waves propagating parallel to the ambient magnetic field, in a dusty plasma, with emphasis on the parametric dependence of the mode-coupling phenomena which have been shown to occur due to the presence of the dust. For this analysis, we consider a range of values of the ambient magnetic field, of the ion

[a)]Electronic mail: ziebell@if.ufrgs.br

temperature, of the ratio between electron and ion temperature, of the ion and dust densities, and of the diameter of the dust particles, assumed to be spherical. This analysis greatly complements the previous analysis.[1] It also shows the possibility of occurrence of coupling between waves in the whistler branch and waves in the branch of circularly polarized waves, due to the presence of the dust particles, a phenomenon not yet reported in the literature, to the best of our knowledge.

The structure of the paper is the following. In Sec. II we briefly outline the model used to describe the dusty plasma. In Sec. III we present essential features of the dielectric tensor to be used in the discussion of wave propagation exactly parallel to the external magnetic field, derived assuming Maxwellian distributions for the electrons and ions in the equilibrium, and the ensuing dispersion relation. In Sec. IV the numerical results obtained from the dispersion relation modified by the dust are presented and discussed. The conclusions are presented in Sec. V.

II. THE DUSTY PLASMA MODEL

We consider a plasma in a homogeneous external magnetic field $\mathbf{B_0}=B_0\mathbf{e_z}$. In this magnetized plasma we take into account the presence of spherical dust grains with constant radius a and variable charge q_d; this charge originates from inelastic collisions between the dust particles and particles of species β (electrons and ions), with charge q_β and mass m_β. For simplicity, we will consider simply charged ions.

The charging model for the dust particles must in principle take into account the presence of an external magnetic field. This field must influence the characteristics of charging of the dust particles, because the path described by electrons and ions is modified: in this case we have cyclotron motion of electrons and ions around the magnetic field lines. However, it has been shown by Chang and Spariosu, through numerical calculation, that for $a \ll \rho_G$, where $\rho_G = (\pi/2)^{1/2} r_{Le}$ and r_{Le} is the electron Larmor radius, the effect of the magnetic field on the charging of the dust particles can be neglected.[20] For the values of parameters used in the present work the relation $a \ll \rho_G$ is always satisfied.

We will consider the dust grain charging process to occur by the capture of plasma electrons and ions during inelastic collisions between these particles. Since the electron thermal speed is much larger than the ion thermal speed, the dust charge will be preferentially negative. As a cross-section for the charging process of the dust particles, we use expressions derived from the OML theory (orbital motion limited theory).[21,22]

In the present work we focus our attention on low-frequency waves in a weakly coupled dusty magnetoplasma, where the electrostatic energy of the dust particles is much smaller than their kinetic energy. This condition allows for a wide variety of natural and laboratory plasmas, with the exception of the so-called colloidal plasmas.[23,24] Dust particles are assumed to be immobile, because of their mass which is much larger than the masses of ions and electrons, and consequently the validity of the proposed model will be restricted to waves with frequency much higher than the characteristic dust frequencies, excluding the modes that can arise from the dust dynamics. More particularly, we will consider the regime in which $|\Omega_d| \ll \omega_{pd} < \omega \leqslant \Omega_i \ll |\Omega_e|$, where Ω_d and Ω_β are the cyclotron frequencies of the dust particles and of electrons and ions, respectively, and ω_{pd} is the plasma frequency of the dust particles. The regime of frequencies $\omega \leqslant \Omega_i$ deserves special attention because it covers the range of the Alfvén waves, although nothing in the formalism prevents the analysis of waves with $\omega > \Omega_i$.

As we will see, in this range of frequencies the dust particles modify the dispersion relation, through modifications of the quasi-neutrality condition and through effects due to dust charge fluctuation. These dust charge fluctuations provide an additional damping mechanism for the Alfvén waves, beyond the well-known Landau damping mechanism.

The dielectric tensor for a magnetized dusty plasma, homogeneous, fully ionized, with identical immobile dust particles and charge variable in time, can be written in the following way:

$$\epsilon_{ij} = \epsilon_{ij}^C + \epsilon_{ij}^N, \tag{1}$$

where the explicit expressions for ϵ_{ij}^C and ϵ_{ij}^N are given in Refs. 18 and 19 and also in the Appendix of Ref. 1.

The term ϵ_{ij}^C is formally identical, except for the $i3$ components, to the dielectric tensor of a magnetized homogeneous conventional plasma of electrons and ions, with the resonant denominator modified by the addition of a purely imaginary term which contains the collision frequency of electrons and ions with the dust particles. For the $i3$ components of the dielectric tensor, in addition to the term obtained with the prescription above, there is a term which is proportional to the inelastic collision frequency of electrons and ions with the dust particles.

The term ϵ_{ij}^N is entirely new and only exists in the presence of dust particles with variable charge. Its form is strongly dependent on the model used to describe the charging process of the dust particles.

III. PROPAGATION PARALLEL TO B_0 AND MAXWELLIAN DISTRIBUTION FUNCTION

If $f_{\beta 0}$ is a Maxwellian distribution the effects of charge variation in the term ϵ_{ij}^C of Eq. (1) only occur in the resonant denominator, being this result independent of the direction of $\mathbf{k}$. The resonant denominator is modified by the addition of a purely imaginary term which contains the inelastic collision frequency of electrons and ions with dust particles. On the other hand, in the case of propagation exactly parallel to the external magnetic field, the term ϵ_{ij}^N appearing in Eq. (1), only occurs for $i=j=3$, regardless of the detailed form of the distribution function $f_{\beta 0}$.

As a consequence, in the case of propagation parallel to the external magnetic field and Maxwellian distributions for the electrons and ions, the dielectric tensor assumes the form

$$\vec{\vec{\epsilon}} = \begin{pmatrix} \epsilon_{11}^C & \epsilon_{12}^C & 0 \\ -\epsilon_{12}^C & \epsilon_{11}^C & 0 \\ 0 & 0 & \epsilon_{33}^C + \epsilon_{33}^N \end{pmatrix}, \tag{2}$$

where

$$\epsilon_{11}^C = 1 + \frac{1}{4}\sum_\beta X_\beta[\hat{I}_\beta^+ + \hat{I}_\beta^-],$$

$$\epsilon_{12}^C = -\frac{i}{4}\sum_\beta X_\beta[\hat{I}_\beta^+ - \hat{I}_\beta^-],$$

$$\epsilon_{33}^C = 1 + \sum_\beta X_\beta \hat{I}_\beta^0,$$

and where

$$\hat{I}_\beta^s \equiv \frac{1}{n_{\beta 0}}\int d^3p \frac{p_\perp \partial f_{\beta 0}/\partial p_\perp}{1 - \frac{k_\parallel p_\parallel}{m_\beta \omega} + s\frac{\Omega_\beta}{\omega} + i\frac{\nu_{\beta d}^0(p)}{\omega}},$$

$$\hat{I}_\beta^0 \equiv \frac{1}{n_{\beta 0}}\int d^3p \frac{p_\perp (p_\parallel/p_\perp)^2 \partial f_{\beta 0}/\partial p_\perp}{1 - \frac{k_\parallel p_\parallel}{m_\beta \omega} + i\frac{\nu_{\beta d}^0(p)}{\omega}},$$

with

$$\nu_{\beta d}^0(p) = \frac{\pi a^2 n_{d0}}{m_\beta}\frac{(p^2 + C_\beta)}{p}H(p^2 + C_\beta),$$

$$X_\beta = \frac{\omega_{p\beta}^2}{\omega^2}, \quad \omega_{p\beta}^2 = \frac{4\pi n_{\beta 0} q_\beta^2}{m_\beta}, \quad \Omega_\beta = \frac{q_\beta B_0}{m_\beta c},$$

$$C_\beta = -\frac{2 q_\beta m_\beta q_{d0}}{a},$$

and $s = \pm 1$. The subscript $\beta = e, i$ identifies electrons and ions, respectively, $q_{d0} = \varepsilon_d e Z_d$ is the equilibrium charge of the dust particles (positive, $\varepsilon_d = +1$, or negative, $\varepsilon_d = -1$) and H denotes the Heaviside function. The number of charges in each dust particle, Z_d, is calculated from the equation of balance of current in the dust particles, in the equilibrium state, and from the quasi-neutrality condition, which gives also n_{e0} if we fix the ion and dust densities n_{i0} and n_{d0}. The explicit form of the quantity ϵ_{33}^N is not necessary for the present investigation and therefore will not be reproduced here.[1,18,19]

The general dispersion relation for $\mathbf{k} = k_\parallel \mathbf{e_z}$ and Maxwellian distributions for electrons and ions therefore follows from the determinant

$$\det\begin{pmatrix} \epsilon_{11}^C - N_\parallel^2 & \epsilon_{12}^C & 0 \\ -\epsilon_{12}^C & \epsilon_{11}^C - N_\parallel^2 & 0 \\ 0 & 0 & \epsilon_{33}^C + \epsilon_{33}^N \end{pmatrix} = 0. \tag{3}$$

In this expression, $N_\parallel = k_\parallel c/\omega$ is the refractive index in the direction parallel to the external magnetic field. The dispersion relation for Alfvén waves is obtained retaining only the components in the upper left 2×2 determinant in Eq. (3), that is, by imposing $E_z = 0$. As a result, we obtain

$$[N_\parallel^2]_s = 1 + \frac{1}{2}\sum_\beta X_\beta \hat{I}_\beta^s, \tag{4}$$

where we have used the expressions for ϵ_{11}^C and ϵ_{12}^C, from Eq. (2).

The effect of the dust particles on the dispersion relation given by Eq. (4) occurs via the quasi-neutrality condition ($n_{i0} \neq n_{e0}$), and also via the dust charge fluctuation present in terms which contain the inelastic collision frequency $\nu_{\beta d}^0$. Following the same procedure used in Ref. 1, for evaluation of the integrals $\hat{I}_\beta^s$, we replace the functions $\nu_{\beta d}^0(p)$ by their average values in momentum space,

$$\nu_\beta \equiv \frac{1}{n_{\beta 0}}\int d^3p\, \nu_{\beta d}^0(p) f_{\beta 0}. \tag{5}$$

In the case of Maxwellian distributions, the average collision frequencies can be written as follows:

$$\nu_i = 2\sqrt{2\pi} a^2 n_{d0} v_{Ti}(1 + \chi_i),$$

$$\nu_e = 2\sqrt{2\pi} a^2 n_{d0} v_{Te} e^{\chi_e},$$

where $\chi_i \equiv Z_d e^2/(aT_i)$, $\chi_e \equiv -(T_i/T_e)\chi_i$, and $v_{T\beta} = (T_\beta/m_\beta)^{1/2}$.

Using these average collision frequencies and performing the calculation of the I_β^s integrals, the dispersion relation given by equation (4) assumes the form

$$[N_\parallel^2]_s = 1 + \sum_\beta X_\beta \zeta_\beta^0 Z(\hat{\zeta}_\beta^s), \tag{6}$$

where Z is the plasma dispersion function,[25] defined by

$$Z(\zeta) = \frac{1}{\sqrt{\pi}}\int_{-\infty}^{+\infty} dt \frac{e^{-t^2}}{t - \zeta},$$

and

$$\zeta_\beta^0 \equiv \frac{\omega}{\sqrt{2} k_\parallel v_{T\beta}}, \quad \hat{\zeta}_\beta^s \equiv \frac{\omega + s\Omega_\beta + i\nu_\beta}{\sqrt{2} k_\parallel v_{T\beta}}.$$

In the absence of dust and for the conditions of existence of Alfvén waves, this dispersion relation collapses into a single branch, reproducing the well-known dispersion relation for an electron-ion plasma.

At this point it is useful to prepare the dispersion relation for the numerical solution, introducing the following dimensionless quantities:

$$z = \frac{\omega}{\Omega_i}, \quad \delta = \frac{n_{i0}}{n_{e0}}, \quad \epsilon = \frac{n_{d0}}{n_{i0}},$$

$$u_\beta = \frac{v_{T\beta}}{v_A}, \quad \gamma = \frac{\lambda^2 n_{i0} v_A}{\Omega_i}, \quad a = \lambda \tilde{a},$$

$$\lambda = \frac{e^2}{T_i}, \quad \tau_e = \frac{T_e}{T_i}, \quad q = \frac{k_\parallel v_A}{\Omega_i},$$

$$\tilde{\nu}_\beta = \frac{\nu_\beta}{\Omega_i}, \quad \eta_\beta = \frac{\omega_{p\beta}}{\Omega_i}, \quad r_\beta = \frac{\Omega_\beta}{\Omega_i}, \tag{7}$$

where v_A is the Alfvén velocity,

$$v_A^2 = \frac{B_0^2}{4\pi n_{i0} m_i}.$$

The relevant results can therefore be cast in terms of these dimensionless quantities. For instance, the dimensionless collision frequencies are given by

$$\tilde{\nu}_i = 2\sqrt{2\pi}\epsilon\gamma\tilde{a}^2 u_i(1+\chi_i),$$

$$\tilde{\nu}_e = 2\sqrt{2\pi}\epsilon\gamma\tilde{a}^2 u_e e^{\chi_e}, \tag{8}$$

where $\chi_i = Z_d/\tilde{a}$ and $\chi_e = -\chi_i/\tau_e$.

The dispersion relation becomes, in terms of these dimensionless quantities,

$$\frac{q^2c^2}{v_A^2 z^2} = 1 + \sum_\beta \frac{\eta_\beta^2}{\sqrt{2}qu_\beta z} Z(\hat{\zeta}_\beta^s), \tag{9}$$

where

$$\hat{\zeta}_\beta^s = \frac{z + sr_\beta + i\tilde{\nu}_\beta}{\sqrt{2}qu_\beta}.$$

IV. NUMERICAL ANALYSIS

In the present section we present a parametric study of the solutions of the dispersion relation given by Eq. (9). Along the study we change several important parameters, considering as basic parameters the ion charge number $Z_i = 1.0$ and the ion mass $m_i = m_p$, where m_p is the proton mass. For the classical distance of minimum approach, measured in cm, we use the value $\lambda = 1.44\times10^{-7}/T_i(\mathrm{eV})$, where $T_i(\mathrm{eV})$ means the ion temperature expressed in units of eV. We choose the ambient magnetic field $B_0 = 1.0\times10^{-4}$ T, ion density $n_{i0} = 1.0\times10^9$ cm^{-3}, ion temperature $T_i = 1.0\times10^4$ K, and electron temperature $T_e = T_i$. For the radius of the dust particles, we assume $a = 1.0\times10^{-4}$ cm. These parameters may be representative of plasmas in stellar winds. They are the same utilized in Ref. 1, where it is possible to find reference to some sources which discuss the motivations for the study of Alfvén waves in stellar wind plasmas, and justify the choice of parameters.

We start by investigating Eq. (9) in the range of small values of dust density, considering ϵ between 0 and 5.0×10^{-6}. As it is known, in the limit $\epsilon = 0$, ion and electron densities are equal and $\tilde{\nu}_e = \tilde{\nu}_i = 0$, and therefore the dispersion relation becomes the usual dispersion relation for Alfvén waves in the absence of dust.

We start the analysis with the display of two figures which have already appeared in Ref. 1. They are repeated here because of their usefulness for the identification of the modes predicted by the dispersion relation. In Fig. 1 we observe the real part of the two roots obtained from Eq. (9) for each of the signs $s = 1$ and $s = -1$. There are two curves with positive values of z_r, describing waves propagating in the positive direction. The uppermost curve is obtained with $s = 1$, and corresponds to the so-called *whistler* branch, while the lower curve in the positive side is obtained with $s = -1$ and corresponds to the branch identified with circularly polarized waves propagating along the ambient magnetic field. These curves have already appeared in our previous work,[1] and are easily recognized from well-known textbooks.[26] For negative values of z_r we have perfectly symmetrical solutions propagating in negative direction, obtained, respectively, with $s = 1$ (the upper curve, closer to the axis) and $s = -1$ (the lower curve). For small values of q, $q \leqslant 0.2$, the two branches of waves propagating in a given direction collapse together in a single branch known as the branch of the Alfvén waves. Each of the curves appearing in Fig. 1 corresponds to the superposition of five curves, obtained with $\epsilon = 0.0$, 1.25×10^{-6}, 2.50×10^{-6}, 3.75×10^{-6} and 5.0×10^{-6}. These results show that the presence of a small density of dust particles has negligible effect on the real part of the roots obtained from the dispersion relation of low-frequency waves propagating along the magnetic field.

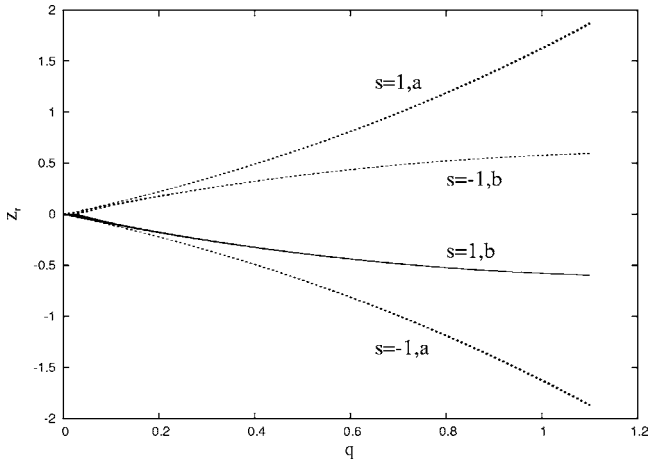

FIG. 1. Real part of the normalized frequency (z_r) for the two roots obtained using $s = 1$ and for the two roots obtained using $s = -1$, as a function of q, for five values of ϵ: $B_0 = 1.0\times10^{-4}$ T, $T_i = 1.0\times10^4$ K, $n_{i0} = 1.0\times10^9$ cm^{-3}, $Z_i = 1.0$, $m_i = m_p$, and $T_e = T_i$. The radius of dust particles $a = 1.0\times10^{-4}$ cm. The dust density n_{d0} is obtained from $\epsilon = n_{d0}/n_{i0}$, and the values of ϵ utilized are $\epsilon = 0.0$, 1.25×10^{-6}, 2.50×10^{-6}, 3.75×10^{-6}, and 5.0×10^{-6}. For this range of variation of ϵ, the quantity z_r is almost independent of the dust density, so that the five curves appear superposed (Ref. 1).

In Fig. 2 we see the corresponding imaginary parts. Figure 2(a) shows the imaginary part of the root corresponding to the whistler branch appearing in Fig. 1, either for $s = 1, a$ or $s = -1, a$. It is seen that the damping rate for these waves is negligible in the absence of dust ($\epsilon = 0$), but becomes significant in the presence of even a small amount of dust, especially in the range of small values of q. Figure 2(b) depicts the imaginary part corresponding to the branch of the circularly polarized waves. In the region of small values of q, where the waves are identified with Alfvén waves, the damping rate is negligible for $\epsilon = 0$, becoming significant for q approaching $q = 1$. This damping is due to wave-particle resonance and is known as the ion-cyclotron damping, which occurs for $|\omega| \simeq \Omega_i$. In the presence of dust this mode detaches from the mode depicted in Fig. 2(a). The damping due to the dust particles is relatively small for very small q, becomes significant for larger values of q, and competitive with the ion-cyclotron damping for $q \simeq 1$. Even for $q \simeq 1$, Fig. 2(b) shows that the damping due to dust particles tends to dominate over the ion-cyclotron damping, even for the relatively small dust density which has been considered in the case of Fig. 2.

It is interesting to notice that, in the absence of dust, the

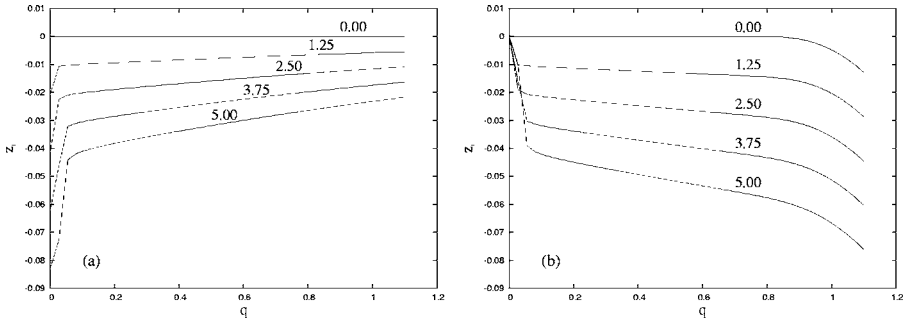

FIG. 2. (a) Imaginary part (z_i) of the positive propagating upper root appearing in Fig. 1, obtained with $s=1$, as a function of q, for the same five values of ϵ used for Fig. 1. (b) Imaginary part (z_i) of the lower positive propagating root appearing in Fig. 1, obtained with $s=-1$, as a function of q, for the same five values of ϵ used for Fig. 1. The labels on the curves indicate $\epsilon=0.0$, 1.25×10^{-6}, 2.50×10^{-6}, 3.75×10^{-6}, and 5.0×10^{-6}. Other parameters are the same as in Fig. 1 (Ref. 1).

damping rate in the range of small q is given analytically by the well-known expression for Landau damping of Alfvén waves,

$$z_i = -\sqrt{\frac{\pi}{8}}\frac{\eta_i^2}{q(1+\eta_i^2)u_i}\exp\left(-\frac{1}{2q^2u_i^2}\right). \tag{10}$$

For the parameters which we are utilizing, $u_i \simeq 0.13$. The exponential factor appearing in Eq. (10) is nearly 1.0 $\times 10^{-79}$ for $q=0.4$, and even smaller for smaller values of q. Landau damping of Alfvén waves is in practice completely negligible for the parameters which we are utilizing, while the damping due to the presence of dust particles may become very significant even for small values of dust-density, as seen in Fig. 2.

Figure 3 displays the values of the real part of the normalized frequency z_r as a function of ϵ, for six values of q

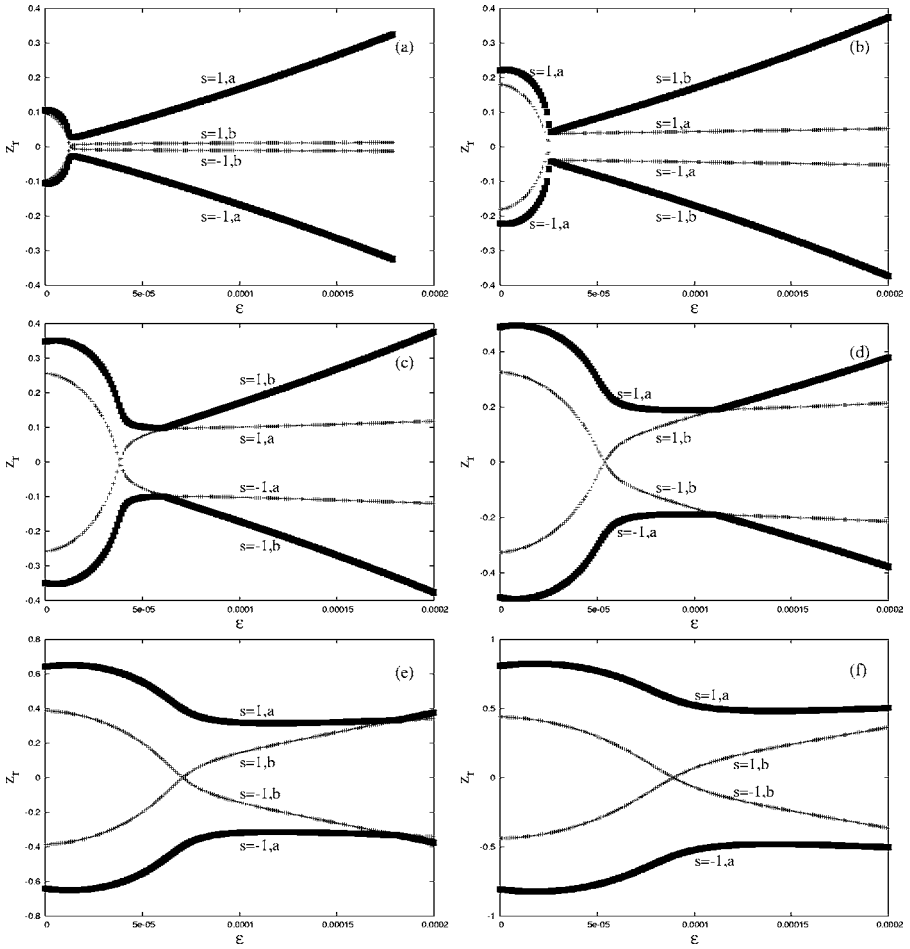

FIG. 3. Real part of the normalized frequencies (z_r) as a function of ϵ, for ϵ between 0.0 and 2.0×10^{-4}, for $s=\pm1$, and six values of q. (a) $q=0.1$; (b) $q=0.2$; (c) $q=0.3$; (d) $q=0.4$; (e) $q=0.5$; (f) $q=0.6$. As in Fig. 1, the curves identified as $s=+1,a$ and $s=-1,a$ pertain to the whistler branch in the limit of vanishing dust density, and the curves identified as $s=+1,b$ and $s=-1,b$ pertain to the branch of circularly polarized waves. Other parameters as in Fig. 1.

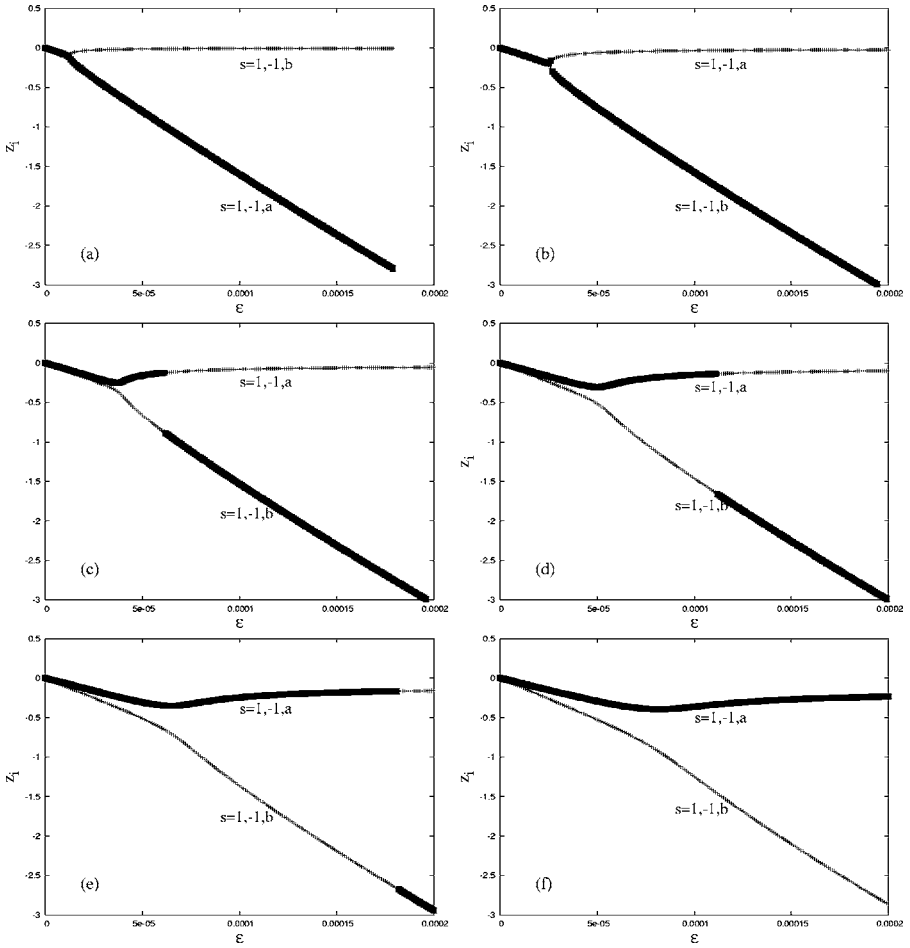

FIG. 4. Imaginary part of the normalized frequencies (z_i) as a function of ϵ, for ϵ between 0.0 and 2.0×10^{-4}, for $s=\pm1$, and six values of q. (a) $q=0.1$; (b) $q=0.2$; (c) $q=0.3$; (d) $q=0.4$; (e) $q=0.5$; (f) $q=0.6$. Other parameters as in Fig. 1.

and both signs $s=+1$ and $s=-1$, considering the same parameters utilized for Fig. 1, but considering ϵ up to 2.0×10^{-4}, much above the maximum value of ϵ considered for Figs. 1 and 2. Figure 4 shows the corresponding values of the imaginary part. The values of q depicted in panels (a) to (f) of the figures are, respectively, $q=0.1$, 0.2, 0.3, 0.4, 0.5, and 0.6. According to what we have learned from Fig. 1, for $\epsilon=0$ the uppermost and lowermost curves for z_r shown in each of the panels of Fig. 3 correspond to the values of z_r for the whistler branch obtained for $s=+1$ and $s=-1$, respectively. The other two curves in each panel pertain to the other mode, the circularly polarized branch.

It is seen from Fig. 3(a) that for $q\simeq0.1$ the two roots corresponding to the whistler branch display decreasing values of $|z_r|$ for increasing dust density, up to a point near $\epsilon\simeq1.3\times10^{-5}$, and then show $|z_r|$ increasing linearly with ϵ. It can be shown that the point of minimum value of $|z_r|$ changes with q, being close to $\epsilon=0.7\times10^{-5}$ for $q=0.05$, 1.3×10^{-5} for $q=0.1$, and 1.9×10^{-5} for $q=0.15$.[1] On the other hand, the two roots corresponding to the circularly polarized waves propagating in positive and negative directions, which are well separated for $\epsilon=0$, feature mode-coupling for increasing dust density. Figure 3(a) shows that the point of mode-coupling approximately corresponds to the point of minimum value of z_r for the whistler branch.

In Fig. 3(b) we see the case of $q=0.2$. As in the case of $q=0.1$, the two roots corresponding to the whistler branch display decreasing values of $|z_r|$ for increasing dust density, up to a certain value of ϵ. However, they meet the curves corresponding to the branch of the circularly polarized waves, something that did not happen for smaller values of q, for the parameters utilized. After this meeting point, at $\epsilon\simeq2.7\times10^{-7}$, the figure shows $|z_r|$ nearly constant with further increase of ϵ, instead of growing as in panel (a). The two roots corresponding to the circularly polarized waves propagating in positive and negative directions still feature mode-coupling for increasing dust density, as in the case of panel (a). The point of coupling for these waves increases as compared to the case of panel (a), being close to $\epsilon=2.4\times10^{-5}$.

Figures 3(c)–3(f) show similar features occurring for increasing values of q. It is seen that the coupling points occur for larger and larger values of ϵ, for increasing values of q, and that the points of coupling, between forward and backward propagating circularly polarized waves and between whistler and circularly polarized waves, are progressively separated with the increase of q.

In Fig. 4 we see the corresponding imaginary parts. For $q=0.1$, Fig. 4(a) shows that the damping of both modes, which is negligible for $\epsilon=0$, increases linearly with the dust density, up to nearly the value of ϵ where the real parts of the

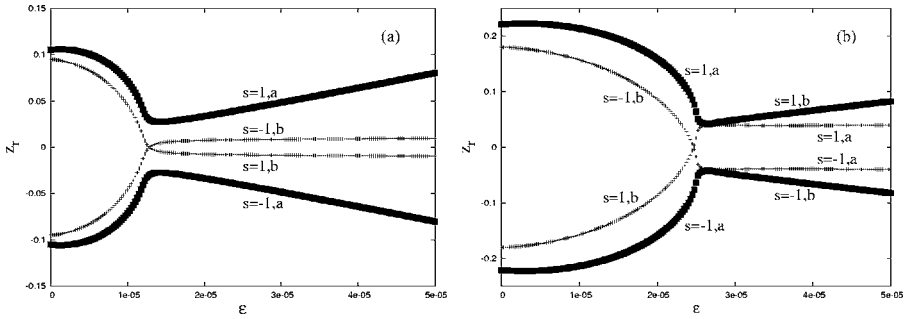

FIG. 5. Real part of the normalized frequencies (z_r) as a function of ϵ, for ϵ between 0.0 and 5.0×10^{-5}, for $s=\pm1$, and two values of q. (a) $q=0.1$; (b) $q=0.2$. Other parameters as in Fig. 1.

two branches show the closest approximation, in Fig. 3(a). Beyond this point, the damping rates of the two modes are separated one from the other. The damping of the waves in the whistler branch continues to increase almost linearly with the dust density, while the damping of the waves in the branch of circularly polarized waves is gradually reduced for increasing values of ϵ. For $q=0.2$ and larger values, Figs. 4(b)–4(f) show behavior qualitatively similar, but with an important difference. For these values of q after the occurrence of mode coupling, it is the branch identified with the cyclotron mode at low ϵ that displays increasing growth rate for increasing values of ϵ, as shown from Figs. 4(b)–4(f). Another qualitative feature to be remarked is that the damping of the two modes becomes progressively more separated even for small values of ϵ, for increasing values of q.

An amplified view of the transition between the situation in which only one coupling point occurs, for $0<q<0.2$, and the situation in which two coupling points occur, for $q\geqslant0.2$, can be seen in Figs. 5 and 6, which show, respectively, the values of z_r and z_i, for $q=0.1$ and $q=0.2$, and for the range of ϵ between 0.0 and 5.0×10^{-5}. This amplified vision shows more clearly the features described in connection with Figs. 3 and 4.

The identification of the roots in Figs. 3 and 4 may be further explained as follows. As we have seen, the coupling point between the whistler branch and the cyclotron branch starts to occur, for the present parameters, at $q\simeq0.2$. Let us consider for example the case of $q=0.3$, in Figs. 3(c) and 4(c). The whistler branch, identified by the bold line in the region of small ϵ, in Fig. 3(c), becomes the thin line after the point of mode coupling. This interpretation is confirmed by the behavior of the imaginary part z_i in Fig. 4(c). The continuity of the curve requires the change of line thickness, from bold to thin. The same requirement applied to the real part in Fig. 3(c) confirms that the real parts of the two branches really cross each other at the point where the curves intercept, and not simply touch each other. Similar features can be seen in panel (b), (d), (e), and (f) of Figs. 3 and 4.

Another view of the complexity of the behavior of the roots of the dispersion relation can be seen in Fig. 7, which shows in panels (a) and (b) the real and imaginary parts of the two roots obtained using $s=1$, as functions of q and ϵ, for q between 0 and 0.3. Corresponding figures can of course be obtained using $s=-1$. The two roots are found by numerical procedures, bold lines are assigned to the root with the higher value of z_r, and thin lines to the root with the lower value of z_r. Figure 7(a) shows that for $\epsilon\rightarrow0$ the root in bold lines is clearly identified with the whistler branch, while the root in thin lines is identified with the cyclotron branch. For $q\leqslant0.2$, the bold plane does not intercept the plane of thin lines. In Fig. 7(b) we see the behavior of z_i, where we easily recognize features already remarked in the comments about Fig. 4(a). For $q\geqslant0.2$, however, Fig. 7(a) shows that the plane in bold lines touches or intercepts the plane in thin lines at a given value of ϵ. Figure 7(b) shows that the continuity of the root requires that the plane in bold must be continued with the plane of thin lines, and vice versa, showing clearly that the real parts indeed cross each other in Fig. 7(a).

The dependence on the ion temperature is shown in Figs. 8 and 9. Figure 8 displays the values of the real part of the normalized frequency z_r as a function of ϵ, for $q=0.4$ and

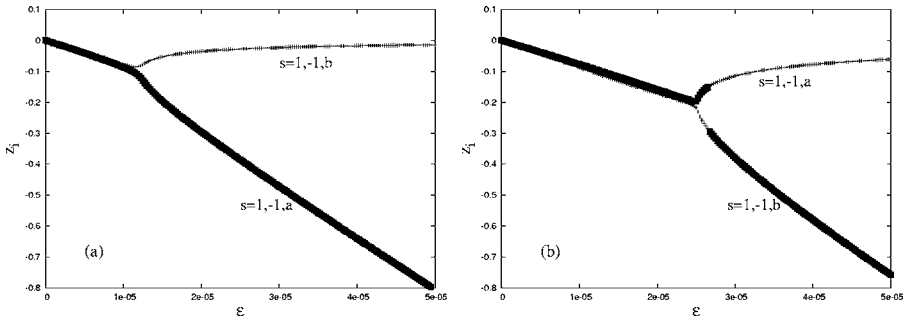

FIG. 6. Imaginary part of the normalized frequencies (z_i) as a function of ϵ, for ϵ between 0.0 and to 5.0×10^{-5}, for $s=\pm1$, and two values of q. (a) $q=0.1$; (b) $q=0.2$. Other parameters as in Fig. 1.

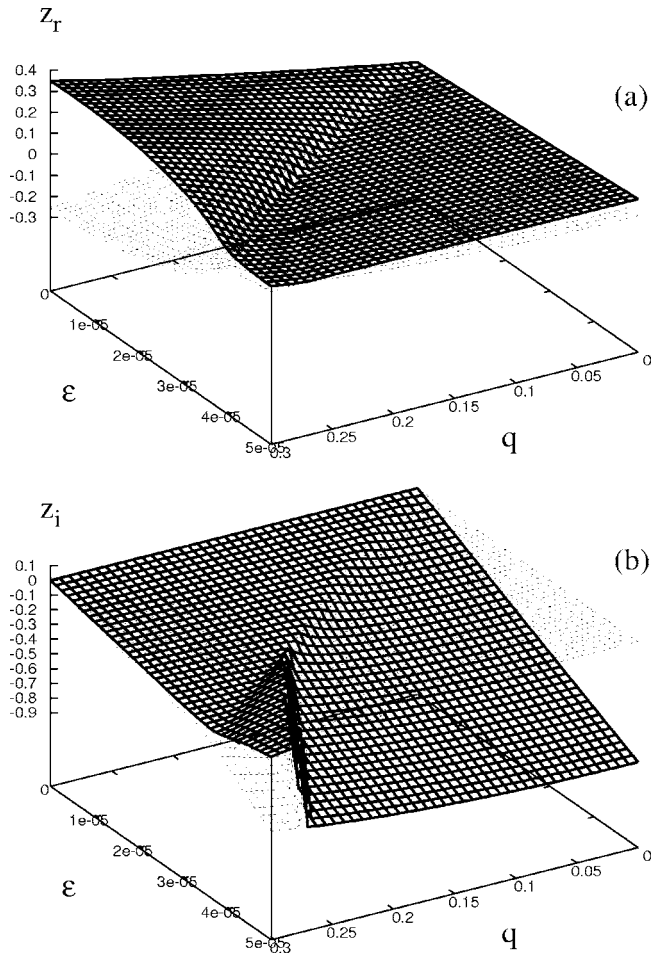

FIG. 7. (a) Combined view of the real parts (z_r) of the two roots obtained with $s=1$, as a function of q and ϵ. (b) Combined view of the imaginary parts (z_i) of the two roots obtained with $s=1$, as a function of q and ϵ. Other parameters are the same as in Fig. 1.

both signs $s=+1$ and $s=-1$, for ϵ up to 2.0×10^{-4}, for several values of ion temperature T_i. We assume in each case $T_e=T_i$. Other parameters are the same as in Fig. 1. The values of T_i used to generate panels (a) to (d) are, respectively, $T_i=0.25\times10^4$ K, 0.5×10^4 K, 2.0×10^4, and 4.0×10^4 K. Figure 8(a) displays the coupling between forward and backward propagating circularly polarized waves appearing near $\epsilon=1.2\times10^{-4}$, while the coupling between whistler and circularly polarized waves do not appear in the range considered in the figure. The successive panels show that the coupling points migrate to smaller values of dust density as the ion temperature is increased. However, the transition between panels (c) and (d) shows that, for sufficiently high ion temperature, the coupling between the whistler branch and the branch of circularly polarized waves ceases to exist, remaining only the coupling between forward and backward circularly polarized waves. One should notice that between the cases depicted in panels (b) and (c) there is the case corresponding to panel (d) in Fig. 3. The corresponding curves for the imaginary part, z_i, appear in Figs. 9(a)–9(d).

The influence of the difference of temperature between electrons and ions is shown in Figs. 10 and 11 for a representative value of the ion temperature. Figure 10 displays the values of z_r as a function of ϵ, for $q=0.4$ and both signs $s=+1$ and $s=-1$, for ϵ up to 2.0×10^{-4}, for several values of the temperature ratio T_e/T_i. The ion temperature is assumed to be $T_i=1.0\times10^4$ K. Other parameters are the same as in Fig. 1. The values of T_e/T_i used to generate panels (a) to (d) are, respectively, $T_e/T_i=0.25$, 0.5, 2.0, and 4.0. Figure 10(a) displays the coupling between forward and backward propagating circularly polarized waves appearing near $\epsilon=1.2\times10^{-4}$, while the coupling between whistler and circularly polarized waves does not appear in the range considered in the figure. The successive panels show that the coupling points migrate to smaller values of dust density as the tem-

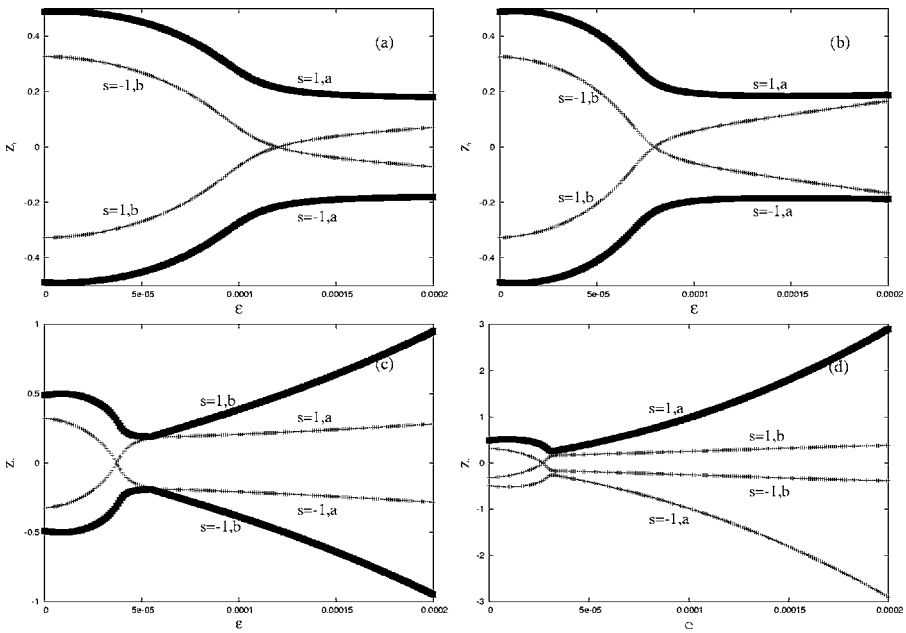

FIG. 8. Real part of the normalized frequencies (z_r) as a function of ϵ, for ϵ between 0.0 and 2.0×10^{-4}, for $s=\pm1$, $q=0.4$, and four values of the ion temperature T_i, for $T_e=T_i$. (a) $T_i=0.25\times10^4$ K; (b) $T_i=0.5\times10^4$ K; (c) $T_i=2.0\times10^4$ K; (d) $T_i=4.0\times10^4$ K. Other parameters as in Fig. 1.

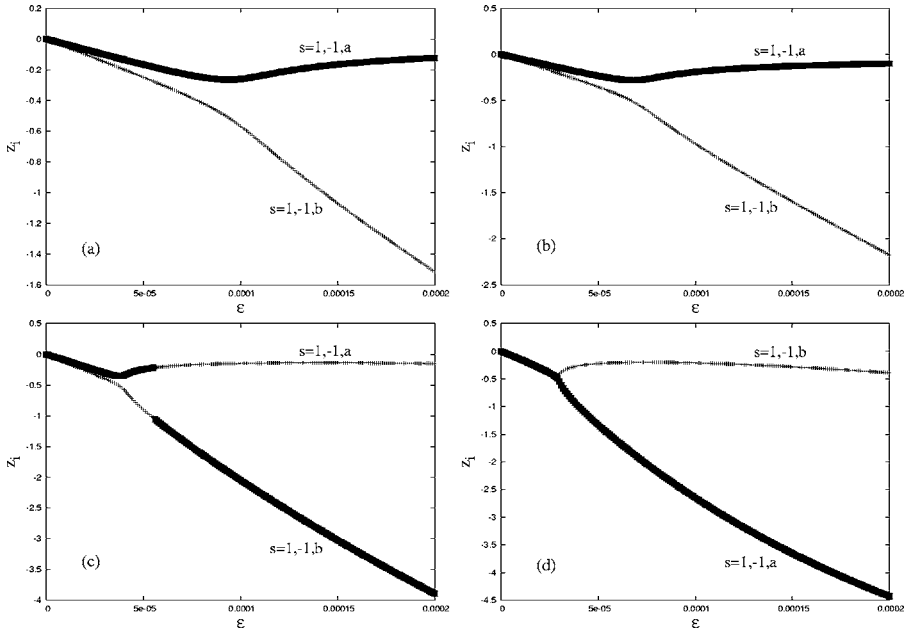

FIG. 9. Imaginary part of the normalized frequencies (z_i) as a function of ϵ, for ϵ between 0.0 and 2.0×10^{-4}, for $s=\pm1$, $q=0.4$, and four values of the ion temperature T_i, for $T_e=T_i$. (a) $T_i=0.25\times10^4$ K; (b) $T_i=0.5\times10^4$ K; (c) $T_i=2.0\times10^4$ K; (d) $T_i=4.0\times10^4$ K. Other parameters as in Fig. 1.

perature ratio is increased. The general appearance of the curves appearing in Figs. 10(a)–10(d) is very similar to those appearing in Figs. 8(a)–8(d), indicating the relevance of the electron temperature for the determination of the behavior of the roots of the dispersion relation for low-frequency waves. However, although the overall similarity, one notices that in the case of $T_e/T_i=4.0$, appearing in Fig. 10(d), the coupling between the whistler branch and the branch of circularly polarized waves continues to occur, while it does not appear in Fig. 8(d), with the same electron temperature, but temperature ratio equal to unity. The corresponding curves for the imaginary part, z_i, appear in Figs. 11(a)–11(d). They are also very similar to the corresponding curves appearing in Figs. 9(a)–9(d).

Figures 12 and 13 show the effect of the radius of the dust particles, considering $T_i=1.0\times10^4$ K, $T_e/T_i=1.0$, and $B_0=1.0\times10^{-4}$ T. Other parameters are the same as in Fig. 1. Figure 12 displays the values of z_r as a function of ϵ, for $q=0.4$ and both signs $s=+1$ and $s=-1$, for ϵ up to 2.0×10^{-4}. The values of a used to generate panels (a) to (d) are, respectively, $a=4.0\times10^{-5}$ cm, 6.0×10^{-5} cm, 8.0×10^{-5} cm, and 1.0×10^{-4} cm. This last value means that Fig. 12(d) is

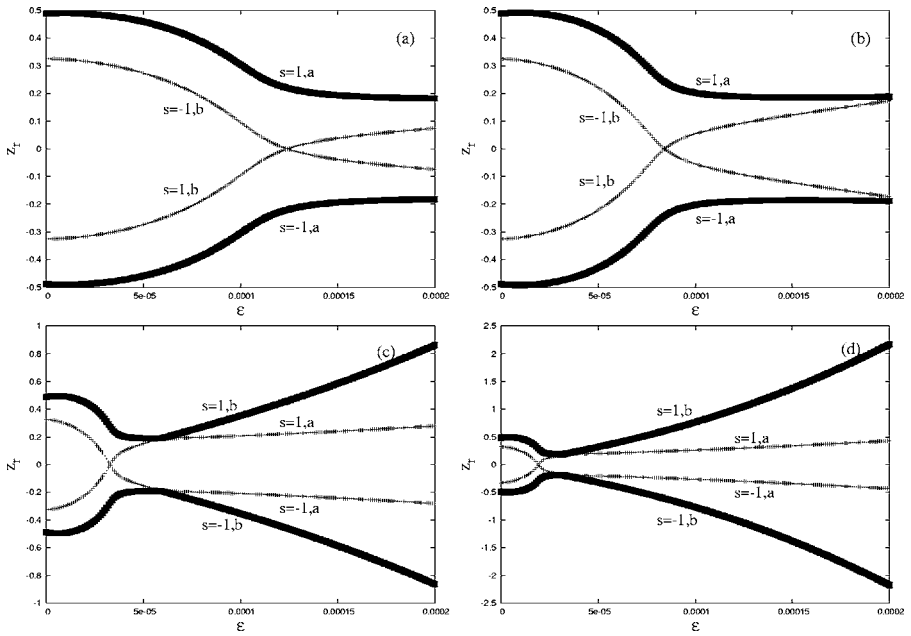

FIG. 10. Real part of the normalized frequencies (z_r) as a function of ϵ, for ϵ between 0.0 and 2.0×10^{-4}, for $s=\pm1$, $q=0.4$, and four values of the ratio T_e/T_i. (a) $T_e/T_i=0.25$; (b) $T_e/T_i=0.5$; (c) $T_e/T_i=2.0$; (d) $T_e/T_i=4.0$. Other parameters as in Fig. 1.

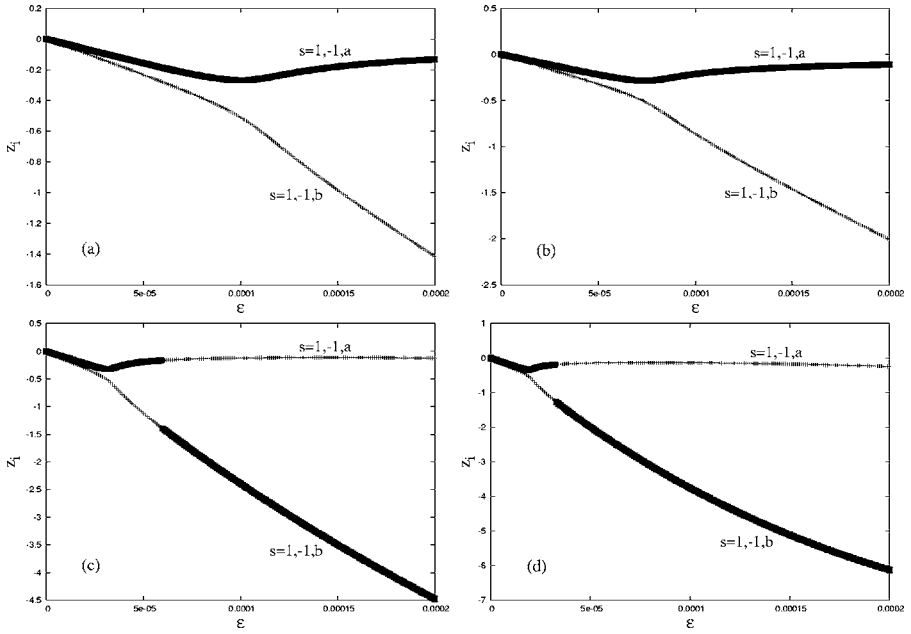

FIG. 11. Imaginary part of the normalized frequencies (z_i) as a function of ϵ, for ϵ between 0.0 and 2.0×10^{-4}, for $s=\pm1$, $q=0.4$, and four values of the ratio T_e/T_i. (a) $T_e/T_i=0.25$; (b) $T_e/T_i=0.5$; (c) $T_e/T_i=2.0$; (d) $T_e/T_i=4.0$. Other parameters as in Fig. 1.

the same as Fig. 3(d). Figure 12(a) shows that the coupling between the roots of the dispersion relation do not appear in the range of the values of ϵ considered for the analysis, in the case of sufficiently small radius of dust particles. For increasing radius, Figs. 12(b)–12(d) show that the couplings occur for progressively smaller values of dust density. It occurs at $\epsilon\simeq1.4\times10^{-4}$ for $a=0.6\times10^{-4}$ cm, $\epsilon\simeq0.8\times10^{-4}$ for $a=0.8\times10^{-4}$ cm, and $\epsilon\simeq0.5\times10^{-4}$ for $a=1.0\times10^{-4}$ cm. This strong dependence of the coupling conditions on the radius of the dust particles poses an interesting question for future analysis, namely, which is the behavior of the wave modes in the case of wave propagation in dusty plasmas with a distribution of particles of different sizes. Such a question, however, is outside of the scope of the present formulation, and shall be addressed in a future investigation. The damping rates corresponding to the cases shown in Figs. 12(a)–12(d) appear in Figs. 13(a)–13(d).

Another parameter to be varied is the intensity of the ambient magnetic field. Figure 14 displays the values of the real part of the normalized frequency z_r as a function of ϵ, for $q=0.4$, both signs $s=+1$ and $s=-1$, and four values of B_0, for ϵ up to 2.0×10^{-4}, with other parameters as in Fig. 1.

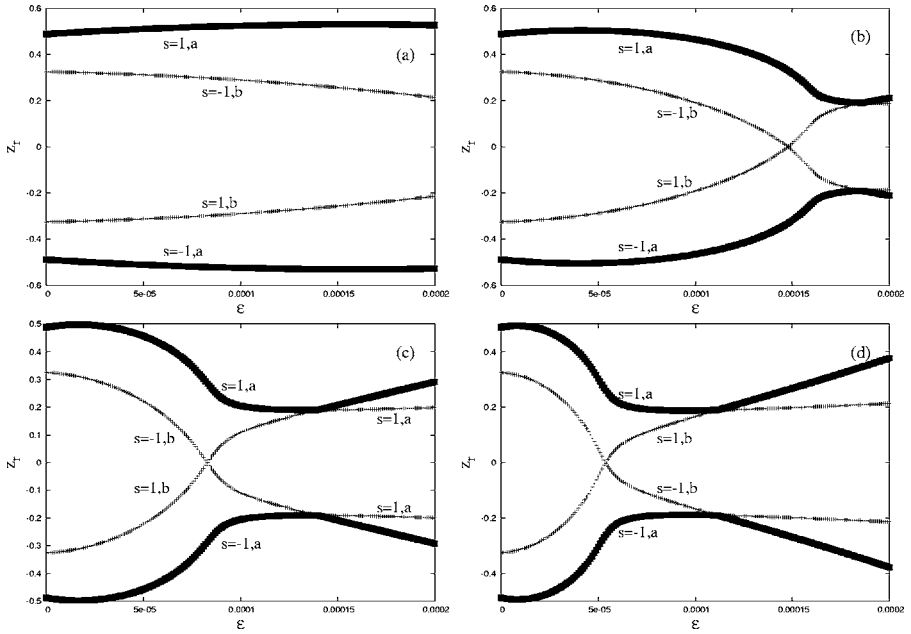

FIG. 12. Real part of the normalized frequencies (z_r) as a function of ϵ, for ϵ between 0.0 and 2.0×10^{-4}, for $s=\pm1$, $q=0.4$, and four values of radius of dust particles, a. (a) $a=4.0\times10^{-5}$ cm; (b) $a=6.0\times10^{-5}$ cm; (c) $a=8.0\times10^{-5}$ cm; (d) $a=1.0\times10^{-4}$ cm. Other parameters as in Fig. 1.

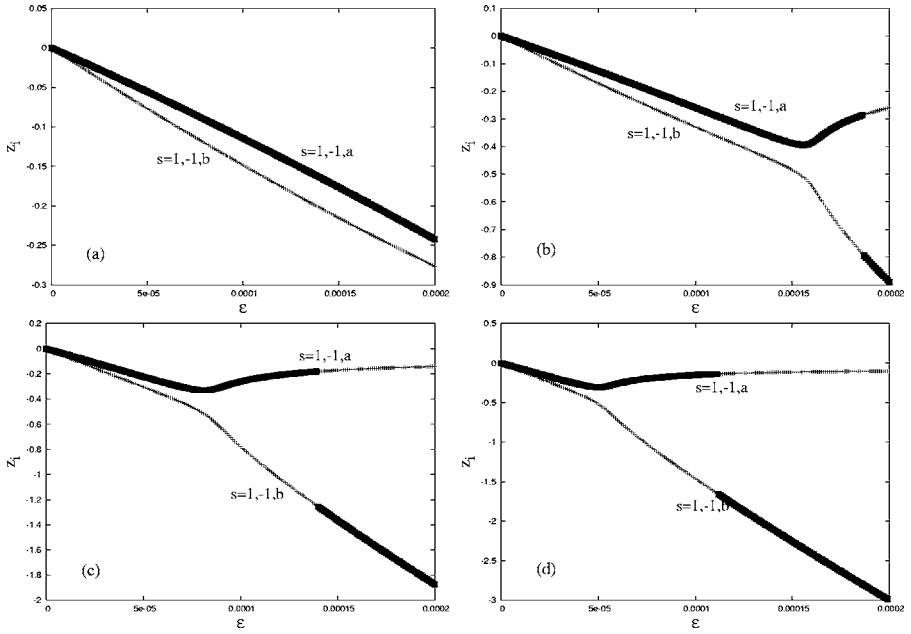

FIG. 13. Imaginary part of the normalized frequencies (z_i) as a function of ϵ, for ϵ between 0.0 and 2.0×10^{-4}, for $s=\pm1$, $q=0.4$, and four values of radius of dust particles, a. (a) $a=4.0\times10^{-5}$ cm; (b) $a=6.0\times10^{-5}$ cm; (c) $a=8.0\times10^{-5}$ cm; (d) $a=1.0\times10^{-4}$ cm. Other parameters as in Fig. 1.

The values of B_0 utilized to generate panels (a) to (d) of Fig. 14 are, respectively, $B_0=1.0\times10^{-4}$ T, 2.0×10^{-4} T, 3.0×10^{-4} T, and 4.0×10^{-4} T. Figure 15 shows the corresponding values of the imaginary part z_i. It is seen from Fig. 14 that the role of the magnetic field is in some sense contrary to the role of the particle diameter. The wave coupling occurs for larger and larger values of ϵ, for increasing magnitude of the magnetic field. The coupling between backward and forward propagating circularly polarized waves, which occurs at $\epsilon\simeq5.0\times10^{-5}$ for $B_0=1.0\times10^{-4}$ T, is moved to $\epsilon\simeq1.8\times10^{-4}$ for $B_0=3.0\times10^{-4}$ T. Moreover, the coupling between the circularly polarized waves and the whistler waves ceases to occur for B_0 approaching 2.0×10^{-4} and above.

The last parameter to be varied in our parametric analysis is the ion density. Figure 16 displays the values of the real part of the normalized frequency z_r as a function of ϵ, for $q=0.4$, both signs $s=+1$ and $s=-1$, and four values of n_{i0}, for ϵ up to 2.0×10^{-4}. The values of n_{i0} utilized to generate panels (a) to (d) of Fig. 16 are, respectively, $n_{i0}=1.0\times10^{9}$ cm^{-3}, 0.50×10^{9} cm^{-3}, 0.25×10^{9} cm^{-3}, and 0.125×10^{9} cm^{-3}. The electron density of course is changed from case to case, as required by the charge neutrality condition.

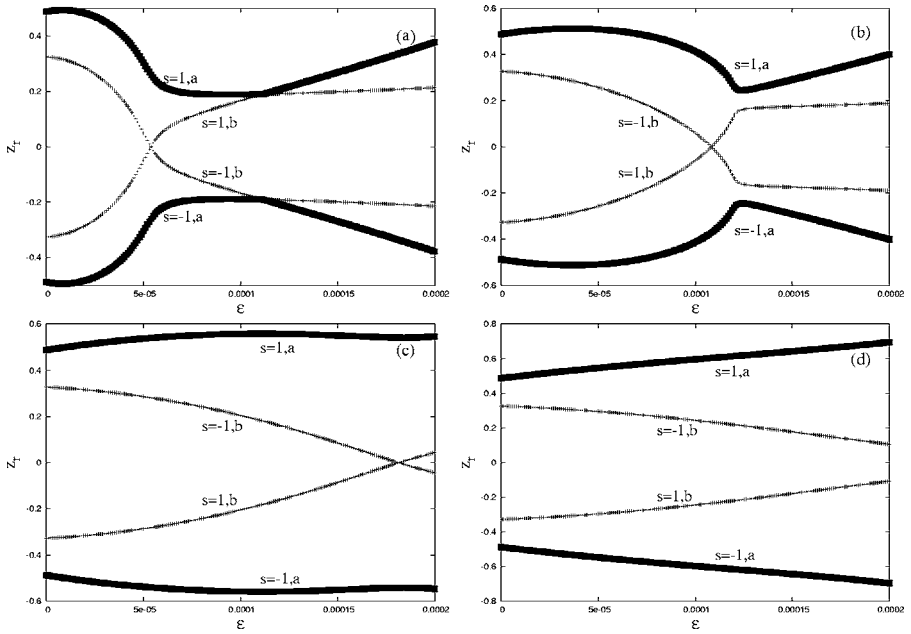

FIG. 14. Real part of the normalized frequencies (z_r) as a function of ϵ, for ϵ between 0.0 and 2.0×10^{-4}, for $s=\pm1$, $q=0.4$, and four values of the magnitude of the ambient magnetic field, B_0. (a) $B_0=1.0\times10^{-4}$ T; (b) $B_0=2.0\times10^{-4}$ T; (c) $B_0=3.0\times10^{-4}$ T; (d) $B_0=4.0\times10^{-4}$ T. Other parameters as in Fig. 1.

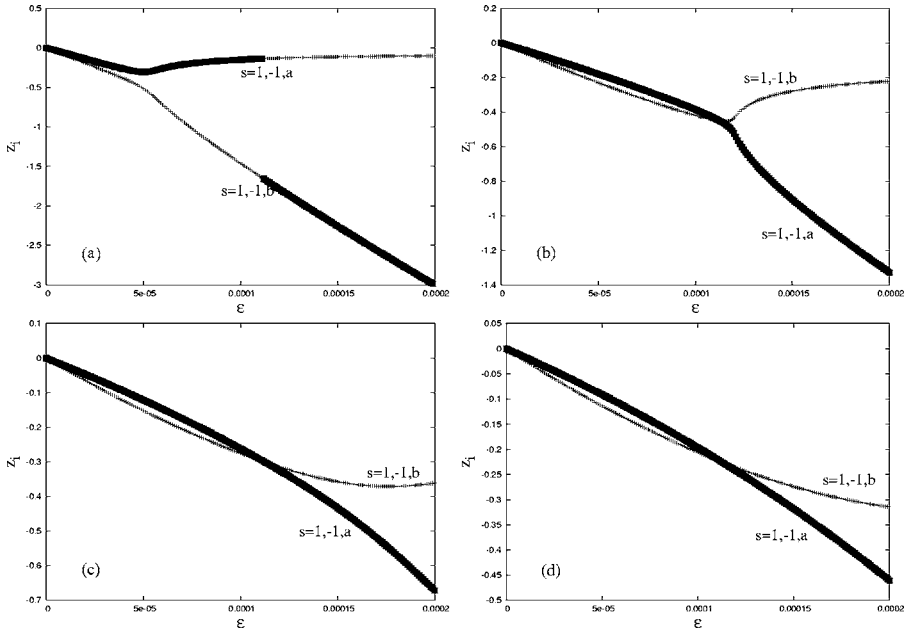

FIG. 15. Imaginary part of the normalized frequencies (z_i) as a function of ϵ, for ϵ between 0.0 and 2.0×10^{-4}, for $s=\pm1$, $q=0.4$, and four values of the magnitude of the ambient magnetic field, B_0. (a) $B_0=1.0\times10^{-4}$ T; (b) $B_0=2.0\times10^{-4}$ T; (c) $B_0=3.0\times10^{-4}$ T; (d) $B_0=4.0\times10^{-4}$ T. Other parameters as in Fig. 1.

Figure 17 shows the corresponding values of the imaginary part z_i. It is seen from Fig. 16, compared to Fig. 14, that the decrease of the ion density causes on the roots of the dispersion relation effect similar to the increase of the magnetic field. The wave coupling occurs for larger and larger values of ϵ, for decreasing ion density.

An interesting feature about the dependence on the ion density can be shown considering the cases depicted in Fig. 18. From the four panels of Fig. 16, we have seen that the characteristics of the wave modes are strongly modified with a reduction by a factor of 8, in the region of relatively small dust density, with ϵ up to 2.0×10^{-4}. In Fig. 18 we see that after the strong modification occurring between the cases of $n_{i0}=1.0\times10^{9}$ cm^{-3} and $n_{i0}=1.0\times10^{8}$ cm^{-3}, a further decrease of two orders of magnitude in the ion density did not change in any meaningful form the characteristics of the quantity z_r. Figure 19 shows similar features appearing in the behavior of the imaginary part z_i.

It may be added that the parameter analysis has been made by changing systematically some important param-

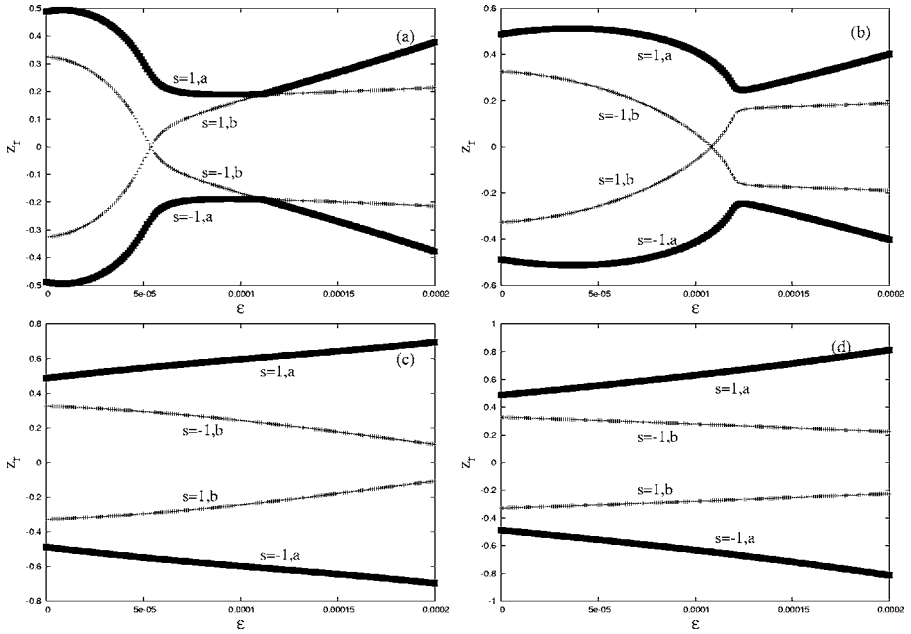

FIG. 16. Real part of the normalized frequencies (z_r) as a function of ϵ, for ϵ between 0.0 and 2.0×10^{-4}, for $s=\pm1$, $q=0.4$, and four values of the ion density, n_{i0}. (a) $n_{i0}=1.0\times10^{9}$ cm^{-3}; (b) $n_{i0}=0.5\times10^{9}$ cm^{-3}; (c) $n_{i0}=0.25\times10^{9}$ cm^{-3}; (d) $n_{i0}=0.125\times10^{9}$ cm^{-3}.

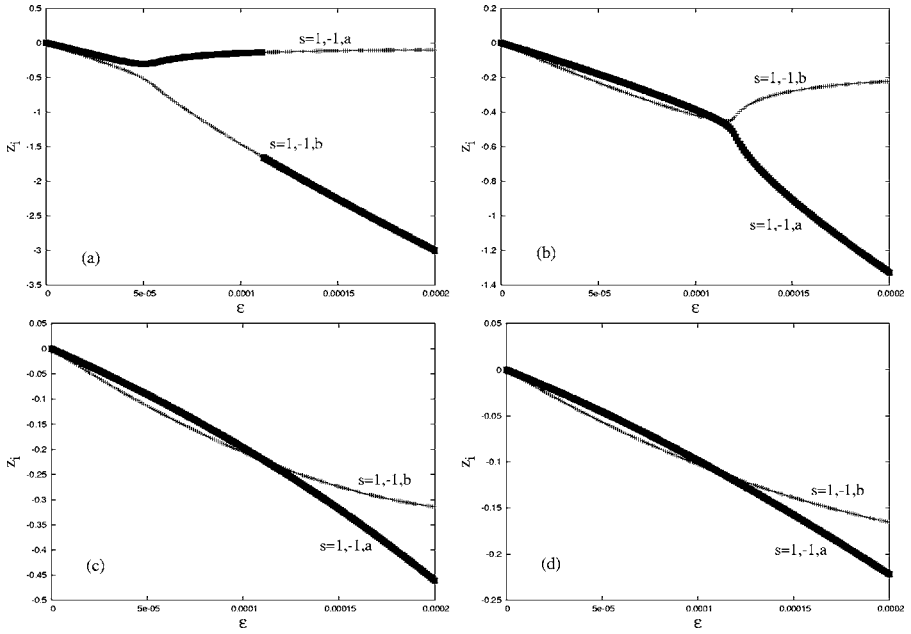

FIG. 17. Imaginary part of the normalized frequencies (z_i) as a function of ϵ, for ϵ between 0.0 and 2.0×10^{-4}, for $s=\pm1$, $q=0.4$, and four values of the ion density, n_{i0}. (a) $n_{i0}=1.0\times10^{9}$ cm^{-3}; (b) $n_{i0}=0.5\times10^{9}$ cm^{-3}; (c) $n_{i0}=0.25\times10^{9}$ cm^{-3}; (d) $n_{i0}=0.125\times10^{9}$ cm^{-3}. Other parameters as in Fig. 1.

eters, using as a starting point the parameters originally used in the analysis of Ref. 1. We have seen, for instance, that the increase of the magnetic field is deleterious to the occurrence of mode coupling in the range of dust densities considered. We have also seen a similar effect due to the decrease of the radius of the dust particles, or due to the decrease in the ion density. These results have been indications about the effect of individual parameters. However, combined effects due to the variation of more than one parameter may occur, extending the range of possibilities for the mode coupling phenomena. It is impossible to consider all possibilities in a paper of reasonable size. As an example, we show in Fig. 20(a) the situation in which the density is given by $n_{i0}=1.0\times10^{8}$ cm^{-3}, and the radius of dust particles is $a=6.0\times10^{-4}$ cm, with the other parameters as in Fig. 1. In Fig. 20(b) we show the case of $n_{i0}=1.0\times10^{8}$ cm^{-3}, and magnetic field intensity $B_0=1.0\times10^{-5}$ T, with the other parameters as in Fig. 1. In both cases we observe the occurrence of mode coupling. The corresponding imaginary parts z_i appear in Fig. 21.

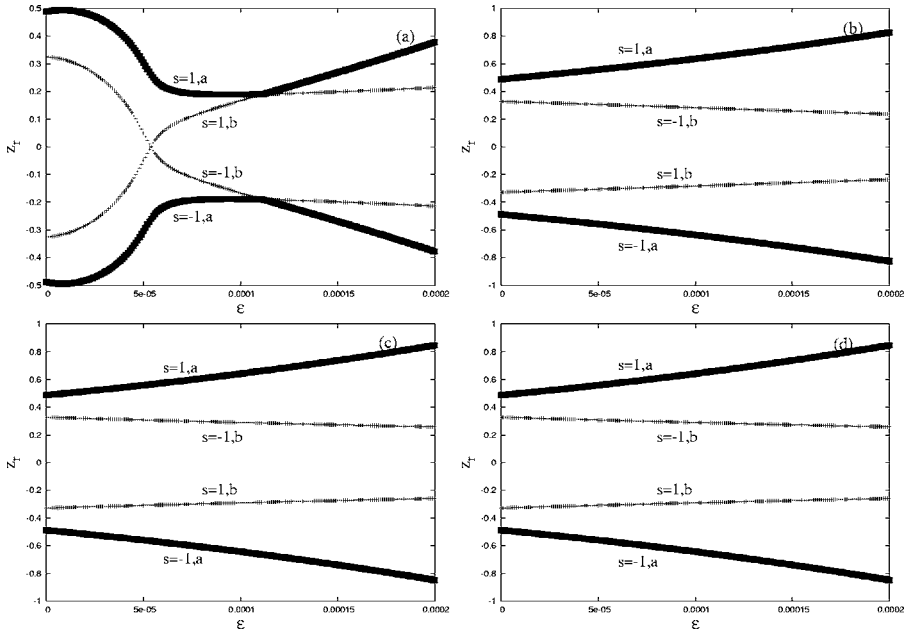

FIG. 18. Real part of the normalized frequencies (z_r) as a function of ϵ, for ϵ between 0.0 and 2.0×10^{-4}, for $s=\pm1$, $q=0.4$, and four values of the ion density, n_{i0}, considering a more extended range than in Fig. 16. (a) $n_{i0}=1.0\times10^{9}$ cm^{-3}; (b) $n_{i0}=1.0\times10^{8}$ cm^{-3}; (c) $n_{i0}=1.0\times10^{7}$ cm^{-3}; (d) $n_{i0}=1.0\times10^{6}$ cm^{-3}. Other parameters as in Fig. 1.

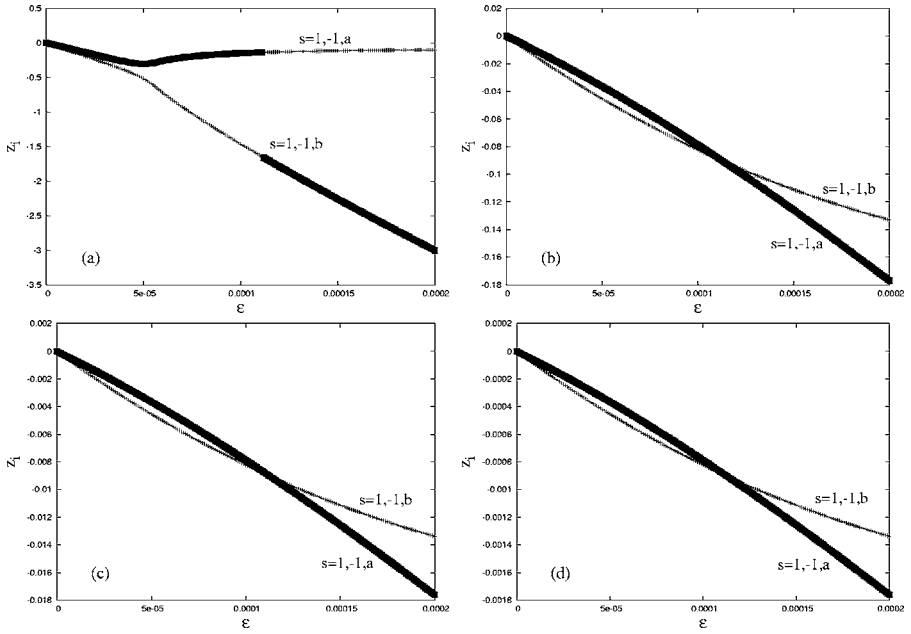

FIG. 19. Imaginary part of the normalized frequencies (z_i) as a function of ϵ, for ϵ between 0.0 and 2.0×10^{-4}, for $s=\pm1$, $q=0.4$, and four values of the ion density, n_{i0}, considering a more extended range than in Fig. 17. (a) $n_{i0}=1.0\times10^{9}$ cm^{-3}; (b) $n_{i0}=1.0\times10^{8}$ cm^{-3}; (c) $n_{i0}=1.0\times10^{7}$ cm^{-3}; (d) $n_{i0}=1.0\times10^{6}$ cm^{-3}. Other parameters as in Fig. 1.

Finally, we add some considerations on the validity of the formalism with the parameters utilized. Let us consider for instance the point of mode coupling occurring in Fig. 3(c), which is close to the value $\epsilon=6.0\times10^{-5}$, and let us assume that the dust particles have mass $m_d\simeq1.0\times5.0\times10^{-11}$ g. This is the value obtained if the dust particles have density similar to that of ice. It may be larger if the dust particles contain material with greater density. For these parameters, $|\Omega_d|/\Omega_i\simeq4.6\times10^{-9}$ and $\omega_{pd}/\Omega_i\simeq8.7\times10^{-2}$. Figure 3(c) shows that the coupling occurs for $z_r\simeq0.11$, therefore the condition $\omega>\omega_{pd}$ is satisfied with a relatively narrow margin, while the condition $\omega\gg\Omega_d$ is satisfied with a very large margin. The validity of the treatment may be in principle compromised in the case of a sufficient reduction of the intensity of the magnetic field, or reduction of the radius of the dust particles, since in both cases the ratio ω_{pd}/Ω_i would be increased, and would be improved in the case of dust particles with larger diameter, or simply larger mass, or in the case of greater intensity of the magnetic field. Consider for instance the case of $a=6.0\times10^{-5}$ cm, shown in Fig. 12(b). It is seen that mode-coupling occurs for $\epsilon\simeq1.7\times10^{-4}$, with $z_r\simeq0.21$. For this value of ϵ, it is found that $\omega_{pd}/\Omega_i\simeq0.23$, which means that the effect of the dust mobility should be taken into account for a better description of the dispersion relation. The same is true for the case of reduced magnetic field, as depicted in Fig. 20(b), in which the values of z_r near the point of mode coupling are also outside the limits of validity of the hypothesis $\omega>\omega_{pd}$. These findings indicate the need for further investigation taking into account the dynamics of the dust particles. We are working on the subject and intend to report our findings in the near future.

V. CONCLUSIONS

In the present paper we have used a kinetic description to analyze wave propagation in dusty plasmas, taking into account the fluctuation of the charge in the dust particles, due to inelastic collisions with electrons and ions. We have considered the case of propagation of waves exactly parallel to

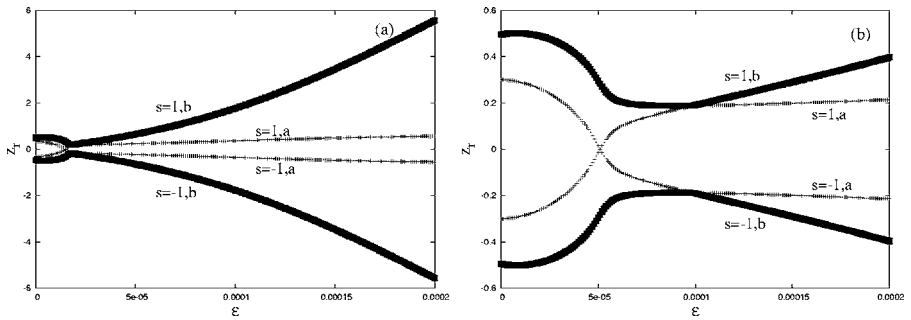

FIG. 20. Real part of the normalized frequencies (z_r) as a function of ϵ, for ϵ between 0.0 and 2.0×10^{-4}, for $s=\pm1$, and $q=0.4$. (a) $n_{i0}=1.0\times10^{8}$ cm^{-3}, $a=6.0\times10^{-4}$ cm; (b) $n_{i0}=1.0\times10^{8}$ cm^{-3}, $B_0=1.0\times10^{-5}$ T. Other parameters as in Fig. 1.

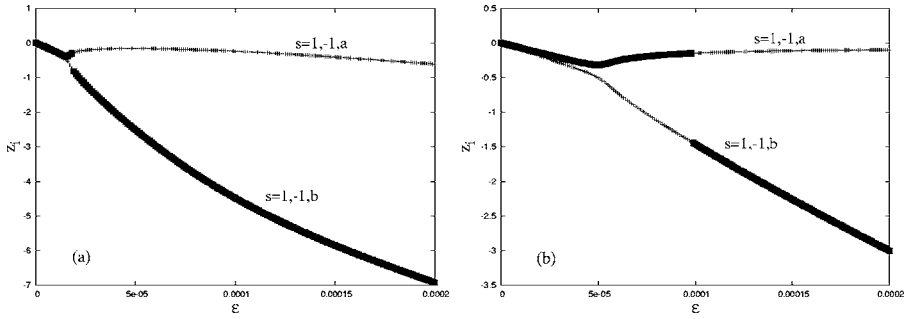

FIG. 21. Imaginary part of the normalized frequencies (z_i) as a function of ϵ, for ϵ between 0.0 and 2.0×10^{-4}, for $s=\pm1$, and $q=0.4$. (a) $n_{i0}=1.0\times10^{8}$ cm^{-3}, $a=6.0\times10^{-4}$ cm; (b) $n_{i0}=1.0\times10^{8}$ cm^{-3}, $B_0=1.0\times10^{-5}$ T. Other parameters as in Fig. 1.

the external magnetic field, and Maxwellian distributions for electrons and ions in the equilibrium situation. We have used this kinetic formulation to obtain and solve the dispersion relation, and perform an analysis of the dependence of the roots of the dispersion relation on several important parameters of the dusty plasma. The emphasis has been on the mode-coupling phenomena which have been previously demonstrated to occur due to the presence of the dust particles.[1]

We have seen that coupling between forward and backward propagating circularly polarized waves may occur at moderately high dust densities, even at the large wavelength limit. For smaller wavelengths, this kind of coupling continues to occur, and coupling between waves in the whistler branch and circularly polarized waves appears for higher dust density. According to the results obtained, the minimum amount of dust required for the coupling to occur increases with the decrease of the wavelength.

The results also show that, for a given wavelength, the coupling points are moved to smaller values of dust density as the ion temperature is increased. Moreover, we have seen that, for sufficiently high ion temperature, the coupling between the whistler branch and the branch of circularly polarized waves may even cease to exist, remaining only the coupling between forward and backward circularly polarized waves.

We have also investigated the effect of temperature difference between electrons and ions, obtaining that the dependence of the roots of the dispersion relation on the parameter T_e/T_i is similar to the dependence of the parameter T_i (for $T_e=T_i$).

The radius of the dust particles has been shown to be very significant for the behavior of the roots of the dispersion relation. For a given wavelength and a given range of values of dust density, we have seen the nonexistence of mode coupling for sufficiently small radius of dust particles. The mode coupling appears for a given value of the radius, and occurs for progressively smaller dust density as the particle's radius is increased. We have also seen that the validity of the hypothesis that the dust dynamics can be neglected may be compromised for sufficiently small dust particles. Of course, these findings pose the question about what would be the behavior of the wave modes in the case of a distribution of particles of different sizes. We intend to address such a question in a future investigation.

We have also investigated the dependence of the wave modes on the intensity of the ambient magnetic field. The results obtained show that the role of the magnetic field is in some sense contrary to the role of the particle diameter. For increasing magnitude of the magnetic field, the wave coupling occurs for increasing values of the parameter ϵ, which increases with the dust density. Moreover, we have seen that the coupling between circularly polarized waves and whistler waves ceases to occur for sufficiently high value of the intensity of the magnetic field. We have also seen that a decrease in the magnetic field intensity may compromise the validity of our hypothesis of immobile dust particles.

Finally, we have investigated the dependence of the wave modes on the ion density. We have seen that the initial decrease of the ion density from our original choice causes on the dispersion relation effect similar to that of the increase of the magnetic field. We have also seen that for the first order of magnitude of decrease in the ion density the wave modes are strongly modified. However, further reduction of two orders of magnitude did not cause further appreciable change, indicating that the solutions of the dispersion relation are relatively independent of the ion density, for that range of densities.

ACKNOWLEDGMENTS

M. C. de Juli was supported by the Brazilian Agency Fundação de Amparo à Pesquisa do Estado de São Paulo (FAPESP) (process number 01/10921-9). L. F. Ziebell and V. Jatenco-Pereira acknowledge support from Brazilian Agency Conselho Nacional de Desenvolvimento Científico e Tecnológico (CNPq).

[1] M. C. de Juli, R. S. Schneider, L. F. Ziebell, and V. Jatenco-Pereira, Phys. Plasmas **12**, 052109 (2005).
[2] W. Pilipp, T. W. Hartquist, O. Havnes, and G. E. Morfill, Astrophys. J. **314**, 341 (1987).
[3] N. N. Rao, J. Plasma Phys. **49**, 375 (1993).
[4] F. Verheest, Space Sci. Rev. **68**, 109 (1994).
[5] F. Verheest and P. Meuris, Phys. Lett. A **210**, 198 (1996).
[6] D. A. Mendis and M. Rosenberg, IEEE Trans. Plasma Sci. **20**, 929 (1992).
[7] D. A. Mendis and M. Rosenberg, Annu. Rev. Astron. Astrophys. **32**, 419 (1994).
[8] P. K. Shukla, Phys. Scr. **45**, 504 (1992).
[9] M. Salimullah, B. D. Gupta, K. Watanabe, and T. Sato, J. Phys. Soc. Jpn. **64**, 3758 (1995).
[10] M. Salimullah and M. Rosenberg, Phys. Lett. A **254**, 347 (1999).
[11] N. Y. Kotsarenko, S. V. Koshevaya, and A. N. Kotsarenko, Phys. Scr. **56**,

388 (1997).
[12]A. C. Das, A. K. Misra, and K. S. Goswami, Phys. Rev. E **53**, 4051 (1996).
[13]P. K. Shukla and H. U. Rahman, Planet. Space Sci. **44**, 469 (1996).
[14]R. V. Reddy, G. S. Lakhina, F. Verheest, and P. Meuris, Planet. Space Sci. **44**, 129 (1996).
[15]V. S. Tsypin, S. V. Vladimirov, A. G. Elfimov, M. Tendler, A. S. de Assis, and C. A. de Azevedo, Phys. Plasmas **4**, 3436 (1997).
[16]M. K. Alam, B. A. Begum, and A. R. Chowdhury, Phys. Plasmas **8**, 4318 (2001).
[17]V. N. Tsytovich and O. Havnes, Comments Plasma Phys. Controlled Fusion **15**, 267 (1993).
[18]M. C. de Juli and R. S. Schneider, J. Plasma Phys. **60**, 243 (1998).
[19]M. C. de Juli and R. S. Schneider, J. Plasma Phys. **64**, 57 (2000).
[20]J. S. Chang and K. Spariosu, J. Phys. Soc. Jpn. **62**, 97 (1993).
[21]J. E. Allen, Phys. Scr. **45**, 497 (1992).
[22]V. N. Tsytovich, Sov. Phys. Usp. **40**, 53 (1997).
[23]G. E. Morfill, H. M. Thomas, U. Konopka, and M. Zuzic, Phys. Plasmas **6**, 1769 (1999).
[24]V. N. Tsytovich, G. E. Morfill, and H. Thomas, Plasma Phys. Rep. **28**, 623 (2002).
[25]B. D. Fried and S. D. Conte, *The Plasma Dispersion Function* (Academic, New York, 1961).
[26]N. A. Krall and A. W. Trivelpiece, *Principles of Plasma Physics* (McGraw-Hill, New York, 1973).